First-principles study of elastic and stability properties of ZrC–ZrN and ZrC–TiC alloys

2009 J. Phys.: Condens. Matter 21 395503

(http://iopscience.iop.org/0953-8984/21/39/395503)

J. Phys.: Condens. Matter **21** (2009) 395503 (8pp) doi:10.1088/0953-8984/21/39/395503

First-principles study of elastic and stability properties of ZrC–ZrN and ZrC–TiC alloys

V I Ivashchenko[1], P E A Turchi[2] and V I Shevchenko[1]

[1] Institute of Problems of Material Science, NAS of Ukraine, Krzhyzhanovsky Street 3, 03142 Kyiv, Ukraine
[2] Lawrence Livermore National Laboratory (L-352), PO Box 808, Livermore, CA 94551, USA

E-mail: ivash@ipms.kiev.ua

Received 6 April 2009, in final form 27 July 2009
Published 8 September 2009
Online at stacks.iop.org/JPhysCM/21/395503

Abstract

Ab initio calculations of the elastic constants for several cubic ordered structures of zirconium carbonitride (ZrC_xN_{1-x}) and zirconium–titanium carbide ($Zr_xTi_{1-x}C$) alloys were carried out. The calculations of total and formation energies, bulk modulus and elastic constants as functions of composition were performed with an *ab initio* pseudo-potential method. The predicted equilibrium lattice parameters are slightly higher than those found experimentally (on average by 0.2–0.4%). The predicted formation energies indicate that the ZrC_xN_{1-x} alloys are stable even at 0 K in the whole concentration range, while the homogeneous $Zr_xTi_{1-x}C$ alloys can be stabilized only at high temperatures. Spinodal decomposition of the latter alloys into cubic domains takes place over a wide range of compositions and temperatures. For the carbonitrides, the shear modulus G, the Young's modulus E and the Poisson ratio σ reach an extremum for carbon-rich alloys, and this is attributed to a maximum value of the shear modulus C_{44} that corresponds to a valence-electron concentration in the range of 8.2–8.3. This extremal behavior finds its origin in the response of the band structure of ZrC_xN_{1-x} alloys for $0 \leqslant x \leqslant 1$, caused by the monoclinic strain that determines this shear modulus. In contrast, the other shear modulus $\frac{1}{2}(C_{11} - C_{12})$ does not exhibit any extremum over the whole composition range. These results are in contrast with those for Zr–Ti carbides for which the elastic properties gradually increase from ZrC to TiC.

1. Introduction

Experimentally, there has been much effort to improve the mechanical properties of transition metal carbides and nitrides by means of alloying metal–metal or non-metal–non-metal elements [1–3]. Along with other transition metal carbonitride and carbide alloys, the ZrC–ZrN and ZrC–TiC systems have attracted considerable interest due to their high hardness and melting temperature and comparatively high electrical and thermal conductivities. As a consequence these alloys are widely used for cutting tools and wear-resistant coatings [4]. Hardness and elastic properties of these alloys have been thoroughly investigated during the last few decades. In short, for the ZrC–ZrN alloys, the following main experimental data were obtained: (i) the lattice parameter of these alloys is a linear function of composition between the carbide and nitride [5]; (ii) there is no ambiguity in determining micro- and nanohardness (H) of zirconium carbonitride as functions of composition. Results on well-characterized specimens [6] show that the hardness of ZrC_xN_{1-x} increases monotonically with x, whereas other results on ZrC–ZrN alloys [7] exhibit a maximum of H at a valence-electron concentration per cell (VEC) of about 8.4; (iii) the bulk modulus (B) shows a slight negative deviation from the mixing rule $B(x) = xB_{ZrC} + (1 - x)B_{ZrN}$ [6] and (iv) the shear (G) and Young (E) moduli exhibit a slight maximum for $x \sim 0.7$ (VEC $\sim$ 8.3) [6].

To the best of our knowledge, there are only a few experimental studies of the structural and mechanical properties of $Zr_xTi_{1-x}C$ alloys [1, 2, 8–10]. In particular, it was established that these alloys exhibit a two-phase mixture in the temperature range of 1400–2000 °C [8, 9] and that the

micro-hardness of the ZrC–TiC system reaches a maximum at intermediate composition [10].

Despite extensive theoretical studies of the electronic structure and elastic properties of transition metal carbide and carbonitride alloys such as, for example, TiC–TiN, HfC–HfN and ZrC–NbC [11–14], so far there are no first-principles calculations of the total energy and elastic constants of the ZrC–ZrN and ZrC–TiC solid solutions. Using a muffin-tin orbital method, Zhukov *et al* [11] have shown that the maximum value of the formation energy of TiC_xN_{1-x} occurs at $x = 0.25$, while pseudo-potential total-energy results [12] indicate a maximum value at $x = 0.75$. Jhi and Ihm [12] also found a positive deviation from the mixing rule for most of the considered structure types. Using an *ab initio* pseudo-potential approach, Jhi *et al* [13] studied the behavior of the shear modulus C_{44} as a function of composition to interpret hardness enhancement in TiC_xN_{1-x}, HfC_xN_{1-x} and $Zr_xNb_{1-x}C$ alloys. The full-potential linearized augmented-plane-wave (FLAPW) method was used to account for the elastic behavior of TiC_xN_{1-x} [14]. The aforementioned theoretical investigations showed that an increase in hardness and elastic constants for Ti and Hf carbonitrides, and $Zr_xNb_{1-x}C$ alloys at intermediate compositions can be attributed to two electronic bands near the Fermi level that shift in opposite directions under shear monoclinic stress [13, 14].

From this brief review we conclude that there are disagreements between some experimental data for ZrC–ZrN systems, and that experimental results for ZrC–TiC alloys are conflicting. We also note that a thorough theoretical investigation of these pseudo-binaries is still lacking. The ZrC–TiC system is based on metals from the same column of the periodic table, which makes it different from other ternary carbide systems that have been theoretically studied [13, 14]. Since the behavior of such materials can be understood on a fundamental level in terms of their electronic band structure, we carried out first-principles calculations of the elastic properties of ZrC_xN_{1-x} and $Zr_xTi_{1-x}C$ to account for the experimental findings available for these alloys, as well as to verify the suggested theoretical models that have been proposed to explain strength enhancement in other similar systems [13, 14]. In the case of $Zr_xTi_{1-x}C$, we also studied the structural stability of this supposedly unstable system [8, 9] with a special emphasis on the temperature effect on alloy stability.

In the present investigation, we performed first-principles density functional theory (DFT) calculations to shed some light on the electronic origin of the strength–composition dependence and the structural stability of ZrC–ZrN and ZrC–TiC systems. *Ab initio* self-consistent pseudo-potential band structure calculations of several cubic ordered structures representing ZrC_xN_{1-x} and $Zr_xTi_{1-x}C$ alloys have been performed. The composition dependence of the lattice parameter a, Gibbs free energy of mixing ΔG_{mix}, elastic constants C_{11}, C_{12} and C_{44}, derived moduli B, G and E, and of the Poisson ratio σ have been predicted and analyzed. The established trends are explained in terms of the modifications, under the corresponding strains, of specific features of the band structure.

2. Computational approach

Scalar-relativistic band structure calculations within the local-density approximation of DFT were carried out using the Quantum-ESPRESSO first-principles code [15] for eight-atom cubic supercells of $Zr_4C_nN_{4-n}$ and $Zr_nTi_{4-n}C_4$, $n = 0, 1, 2, 3, 4$, representing zirconium carbonitride, ZrC_xN_{1-x}, and $Zr_xTi_{1-x}C$ alloys, respectively. Atomic relaxations were neglected, since they were found to be very small with little impact on the behavior of the mechanical properties as functions of composition [12]. Vanderbilt ultra-soft pseudo-potentials were used to describe electron–ion interactions [16]. In the Vanderbilt approach [16], the orbitals are allowed to be as soft as possible in the core regions so that their plane-wave expansion converges rapidly. The semi-core states were treated as valence states. For the zirconium and titanium pseudo-potentials, the nonlinear core corrections were taken into account [15]. To describe exchange–correlation energy, the generalized gradient approximation (GGA) of Perdew *et al* [17] was used. The criterion of convergence for the total energy was 10^{-6} Ryd/formula unit. To speed up convergence, each eigenvalue was convoluted with a Gaussian with a width of 20 mRyd. Since we dealt with different structures, a similar set-up was used for the basis set, tail energies and $\boldsymbol{k}$-point mesh. The cutoff energy for the plane-wave basis was set to 56 Ryd. The integration in the Brillouin zone was done with a number of special $\boldsymbol{k}$-points determined according to the Monkhorst–Pack scheme [18]. We selected the minimal sets of $\boldsymbol{k}$-points (N_k) in the irreducible wedge of the Brillouin zone (BZ) to guarantee that the total energy was changing by no more than 1 mRyd/formula unit by further increasing the number of wavevectors. The following structures were considered: simple cubic ($12 \times 12 \times 12$ grid, $N_k = 84$), orthorhombic ($8 \times 8 \times 8$ grid, $N_k = 125$) and monoclinic ($8 \times 8 \times 8$ grid, $N_k = 170$). No extrapolation to an infinite number N_k was applied. The density of states (DOS) of the strained materials was computed using the following finer k-point meshes: ($10 \times 10 \times 10$ grid, $N_k = 216$) and ($10 \times 10 \times 10$ grid, $N_k = 312$) for the orthorhombic and monoclinic structures, respectively, with a tetrahedron method for integration [15].

The elastic moduli of a cubic crystal may be divided into two classes, the bulk modulus $B = \frac{1}{3}(C_{11} + 2C_{12})$ and the two shear moduli, $C' = \frac{1}{2}(C_{11} - C_{12})$ and C_{44}. The bulk modulus was calculated by fitting the total energy–volume, $E_T(V)$, curve to the traditional Murnaghan equation of state [19]. To calculate the modulus C' we used the volume-conserving orthorhombic strain [14]:

$$\begin{aligned} x' &= (1+\varepsilon)x, \\ y' &= (1+\varepsilon)^{-1}y, \\ z' &= z, \end{aligned} \tag{1}$$

and for the elastic modulus C_{44}, we used the volume-conserving monoclinic strain [14]:

$$\begin{aligned} x' &= x + \gamma y, \\ y' &= y, \\ z' &= z. \end{aligned} \tag{2}$$

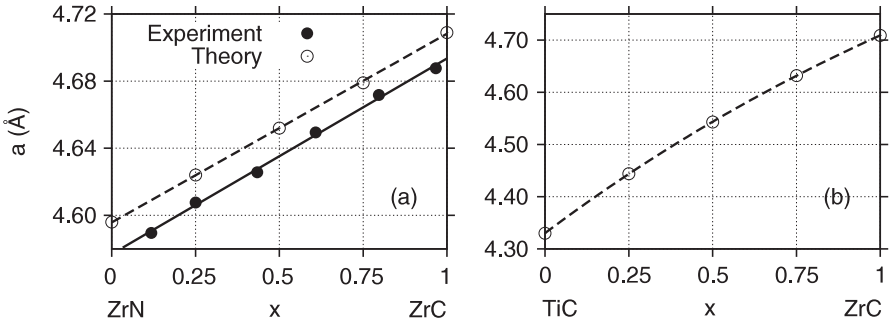

Figure 1. Lattice parameters of ZrC_xN_{1-x} (a) and $Zr_xTi_{1-x}C$ (b) versus composition. Here and in the following figures the solid or dashed line is a polynomial fit to the data points (to be considered as a guide to the eyes).

It should be noted that these strains differ from the strain tensors suggested by Mehl [20]. The strains change the total energy as follows [20]:

$$E_T(V, \delta) = a + b\delta^2 + \mathrm{O}(\delta^4), \tag{3}$$

where V is the volume, a and b are the fitting coefficients, $\delta = \{\varepsilon, \gamma\}$, $b(\varepsilon \to 0) = (C_{11} - C_{12})V$ and $b(\gamma \to 0) = \frac{1}{2}C_{44}V$. Thus, once B, $b(\varepsilon)$ and $b(\gamma)$ are determined, the elastic moduli C_{11}, C_{12} and C_{44} can be calculated. The use of the strains (1) and (2) allowed us to avoid the consideration of tetragonal and trigonal distortions that are sometimes used [21–23].

For the maximal values of the strains ε and γ, we used those suggested in [20]. In particular, we have chosen ε_i and $\gamma_i, i = 1, 2, 3, 4, 5$, and $\varepsilon_5 = 0.05$, $\gamma_5 = 0.07$. The total energy $E_T(i)$ was calculated by taking an average of the computed $E_T(\delta_i)$ over different meshes, weighted by the number of points in the mesh.

Because of symmetry, the $ZrC_{0.5}N_{0.5}$ and $Zr_{0.5}Ti_{0.5}C$ compositions were calculated under the strains ε and γ for three atomic configurations in the non-metal and metal sublattices, respectively. Therefore the resulting elastic moduli for this composition were evaluated as an average value between these configurations.

The band energies associated with the valence band contributions to the total energies were computed according to $E_B = \int E\,N(E)\,\mathrm{d}E$, where $N(E)$ is the DOS, E is the energy and the integration is performed up to the Fermi energy, E_F.

In the case of transition metal compounds, obtained either by hot-pressing [1–3] or by using thin-film technology [4], experiments can only determine the isotropic bulk modulus B and the shear moduli of polycrystalline aggregates of small crystallites. To take into account this fact, we used a scheme suggested by Mehl [20] for the determination of G, E and σ.

The formation energy (ΔE_{Form}) of these alloys was determined as follows:

$$\Delta E_{\mathrm{Form}}(x) = E_T(Zr_xTi_{1-x}C) - x\,E_T(ZrC) - (1-x)\,E_T(TiC), \tag{4}$$

as a function of composition. (For ZrC_xN_{1-x}, a similar expression was considered.) The resulting formation energies were then used to calculate the Gibbs free energies of mixing for $Zr_xTi_{1-x}C$ alloys:

$$\Delta G_{\mathrm{mix}} = \Delta E_{\mathrm{Form}} - T\Delta S, \tag{5}$$

where T is the temperature and ΔS is the configurational entropy for an ideal binary mixture (in our case, the pseudo-binary ZrC–TiC mixture) given by

$$\Delta S = -R[x\ln(x) + (1-x)\ln(1-x)], \tag{6}$$

where R is the ideal gas constant and x is the ZrC mole fraction in $Zr_xTi_{1-x}C$.

3. Results and discussion

In figure 1, we show the concentration dependence of the lattice parameter for ZrC_xN_{1-x} and $Zr_xTi_{1-x}C$ alloys. One can see that, in the case of the carbonitrides, the lattice parameter varies almost linearly with composition, in agreement with the experimental findings [5]. The calculated values slightly exceed the experimental ones (by approximately 0.2–0.4%). For $Zr_xTi_{1-x}C$, we note that the lattice constant (a) shows a slight positive deviation from the mixing rule $a(x) = x \cdot a_{ZrC} + (1-x) \cdot a_{TiC}$, which usually indicates a tendency towards phase separation.

The Gibbs free energy of mixing of ZrC_xN_{1-x}, calculated at 0 K (i.e. formation energy), displayed in figure 2(a) as a function of composition x, indicates that, in the entire composition range, it is energetically favorable for TiC and TiN to mix and form alloys, in agreement with experiment [6]. The polynomial fit to the calculated energies clearly points to a minimum of the formation energy at around $x \sim 0.6$.

In contrast to zirconium carbonitrides, the formation energy of zirconium–titanium carbide alloys is positive in the entire composition range (cf figure 2(b)), which implies that the alloys are not stable, and should decompose into ZrC and TiC compatible with the predicted chemical driving force ΔE_{Form}. However, $Zr_xTi_{1-x}C$ alloys can be stabilized in some range of composition, depending on temperature, since the configurational entropy ΔS (equation (6)) is always positive and promotes a decrease in ΔG_{mix} (equation (5)). We note from figure 2(b) that, at lower temperatures, where $T\Delta S$ is smaller than ΔE_{Form}, ΔG_{mix} develops a negative curvature ($\partial^2 \Delta G_{\mathrm{mix}}/\partial x^2 < 0$) around equi-atomic composition. Here the mixture is not stable for all compositions. Along with this, local minima located at low and high compositions form. These local points defined by the common tangent construction are known as binodal. An increase in temperature leads to a

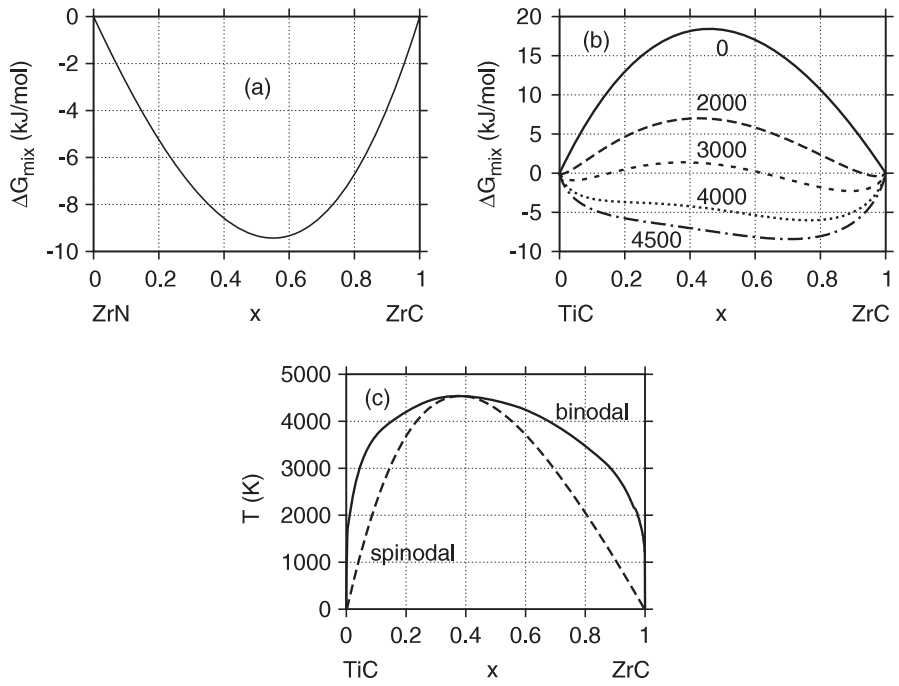

Figure 2. Gibbs free energy of mixing ($\Delta G_{\rm mix}$) versus composition for (a) ZrC_xN_{1-x} at zero temperature and (b) $Zr_xTi_{1-x}C$ at 0, 2000, 3000, 4000 and 4500 K; and (c) calculated temperature–composition phase diagram for $Zr_xTi_{1-x}C$, showing binodal and spinodal with TiC and ZrC chosen as reference states (c).

decrease in the difference between $\Delta E_{\rm Form}$ and $T\Delta S$ and to a coincidence of these local minima at a maximum temperature. Thus, a miscibility gap forms in the phase diagram for $\Delta E_{\rm Form} > T\Delta S$. The binodal line confines the composition–temperature range of instability of the homogeneous mixture. However, it is easy to see that, inside the binodal region, the zones of local stability with respect to small composition fluctuations in the mixture can exist. In such zones, the Gibbs free energy of mixing develops a positive curvature ($\partial^2\Delta G_{\rm mix}/\partial x^2 > 0$). The limit of local stability with respect to small fluctuations is defined by the condition: $\partial^2\Delta G_{\rm mix}/\partial x^2 = 0$ that defines the spinodal line. It is well known that, if $\partial^2\Delta G_{\rm mix}/\partial x^2 < 0$, the mixture is intrinsically unstable and will rapidly separate into two phases by spinodal decomposition, whereas if $\partial^2\Delta G_{\rm mix}/\partial x^2 > 0$, the mixture is metastable and phase separation will take place by nucleation and growth [4]. Figure 2(c) shows the binodal (solid) and spinodal (dashed) lines for $Zr_xTi_{1-x}C$ (inside the spinodal: $\partial^2\Delta G_{\rm mix}/\partial x^2 < 0$). It is clear from figure 2(c) that at room temperature the chemical binodal (spinodal) composition ranges from 0.00 to 1.00 (0.015 to 0.97). The binodal and spinodal lines coincide at a temperature $T \sim 4550$ K and for a composition $x \sim 0.38$. The temperature–composition phase diagram is limited in temperature by melting, or by a possible dissociation into metal and carbon (not considered in the present work). For the sake of comparison, the melting temperatures of ZrC and TiC are about 3800 and 3500 K, respectively [1, 2]. Hence, our results indicate a spinodal decomposition of $Zr_xTi_{1-x}C$ alloys in a wide range of temperatures and compositions, which is consistent with the experimental data available for Zr–Ti carbide films [24]. Based on the phase diagram presented in figure 2(c), one can predict an enhancement of the mechanical properties of the ZrC–TiC system after annealing, caused by the existence of a spinodal decomposition. The latter has been verified in a number of alloy systems and can effectively improve the mechanical properties by providing additional obstacles for dislocation motion, resulting in the well-known precipitation or age-hardening phenomenon [4].

In table 1 we summarize the results of the calculated and experimental elastic constants. For ZrN and ZrC our calculated elastic moduli are in good agreement with the analogous experimental and theoretical data, except with those reported in [21], but this discrepancy can be attributed to the specific procedure that was used to determine the elastic constants. For TiC, we note that our theoretical values of C_{11} and C_{44} agree well with the experimental data [26, 29–31], while the calculated value for C_{12} is higher than the experimental values. As shown in table 1 our results are consistent with those obtained in previous theoretical investigations [12, 14, 28].

The dependence of the shear moduli C' and C_{44} on the VEC are shown in figure 3. For ZrC_xN_{1-x} alloys, the evolution of the shear modulus C' with composition x is monotonic: C' gradually increases with VEC. In contrast, the C_{44} modulus reaches a maximum around VEC ~ 8.3. A different conclusion is drawn for $Zr_xTi_{1-x}C$ alloys: here all the moduli gradually decrease with an increase in ZrC composition, with a negative deviation from the mixture rule. We conclude that, for the TiC–ZrC system, the elastic constants vary monotonically with composition, due to the similarity of their band structures: the Fermi level is located in a minimum of the DOS at all compositions (not shown). The elastic response of such structures to an orthorhombic or a monoclinic strain is expected to be similar.

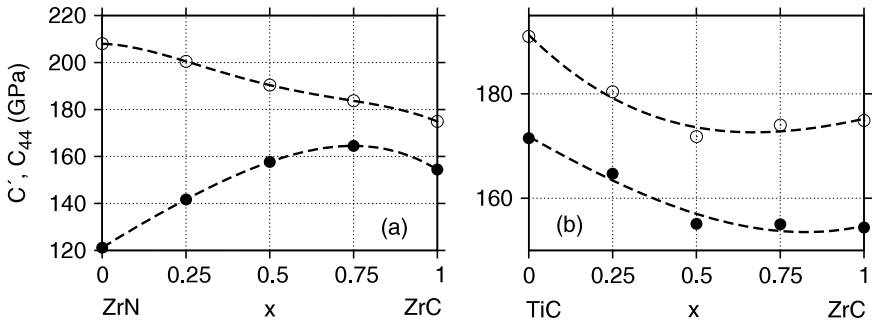

Figure 3. Shear moduli $C' = \frac{1}{2}(C_{11} - C_{12})$ (○) and C_{44} (●) for ZrC_xN_{1-x} (left) and $Zr_xTi_{1-x}C$ (right).

Table 1. Bulk modulus (B) and elastic constants C_{11}, C_{12} and C_{44} (in GPa) of ZrC–ZrN in TiC alloy systems.

Composition	x	B	C_{11}	C_{12}	C_{44}	References
$ZrNi_x$	1.00	245	523	107	121	[a]
	1.00	246	304	114	511	[b]
	1.00	285	611	117	129	[c]
	0.93	232	454	121	124	[d]
ZrC_xN_{1-x}	0.25	239	507	106	142	[a]
	0.50	233	487	106	158	[a]
	0.75	227	472	104	165	[a]
ZrC_x	1.00	219	452	102	154	[a]
	1.00	232	272	134	429	[b]
	1.00	247	522	110	160	[c]
	0.94	223	472	99	150	[e]
	N/A	223	470	100	160	[f]
$Zr_xTi_{1-x}C$	0.75	221	453	105	155	[a]
	0.50	225	454	111	155	[a]
	0.25	233	474	113	165	[a]
TiC_x	1.00	247	502	120	172	[a]
	1.00	247	516	112	166	[g]
	1.00	258	513	130	N/A	[h]
	1.00	221	470	97	167	[i]
	N/A	242	513	106	178	[j]
	0.95	253	540	110	180	[k]
	0.91	242	515	106	179	[e]
	N/A	242	500	113	175	[l]

[a] Self-supporting.
[b] Elastic moduli computed with the FLAPW method [21].
[c] Pseudo-potential results [23, 24].
[d] Elastic constants determined from neutron data [25].
[e] Experimental data [26].
[f] Estimations from phonon dispersion curves [27].
[g] FLAPW data [14].
[h] Pseudo-potential results [12].
[i] GGA-FLAPW results [28].
[j] Experimental values [29].
[k] Results derived from neutron investigations [30].
[l] Results obtained from ultrasonic measurements [31].

To understand the variation of both shear moduli with composition for ZrC_xN_{1-x}, let us analyze the changes in the DOS caused by an orthorhombic and a monoclinic strain. But first let us analyze the DOSs of the unstrained cubic carbonitride phases that are presented in figure 4. We note several changes in the band structure of ZrC, when substituting carbon to nitrogen: (i) the appearance of an additional low-

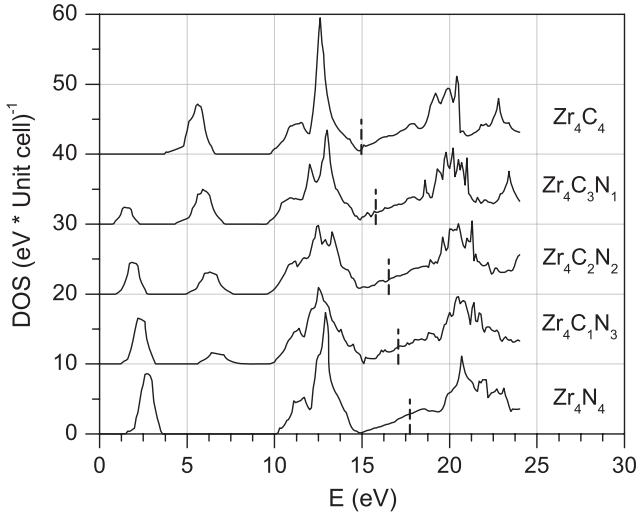

Figure 4. Densities of states (DOS) of cubic $Zr_4C_{4-n}N_n$ ($n = 0, 1, 2, 3, 4$). The vertical dashed line locates the Fermi energy (E_F).

energy peak below 5 eV in the DOS and (ii) a Fermi-level shift towards high energies. An analysis of the partial DOS shows that two low-energy peaks originate from the non-metal s states. The band below the DOS minimum at about 15 eV consists of the non-metal p states and the metal d states (p–d band). Finally, the band above the DOS minimum at about 15 eV originates mostly from the metal d states (d band).

In figure 5 we show the results of the comparison of the DOSs of the unstrained and strained ZrC and ZrN. In the case of the orthorhombic distortion (equation (1)), for both the compounds, a reduction in the lattice parameter a_y causes an appreciable shift of the main peak towards low energies. On the other hand, for ZrC, an increase in a_x gives rise to an increase in the number of states below the energy E_{min} (at about 15 eV) that separates the p–d and d bands. The expansion of the unit cell of ZrN in the x direction leads to the appearance of an additional peak just above E_{min}. The band energies of the distorted structures are slightly lower compared to those of the undistorted ones, which results from a shift of the main peak of the DOS toward low energies. Further inspection of the E_B values did not reveal a distinct correlation between the composition dependence of E_B and C', a fact that can instead be assigned to the difference in the positions of the additional

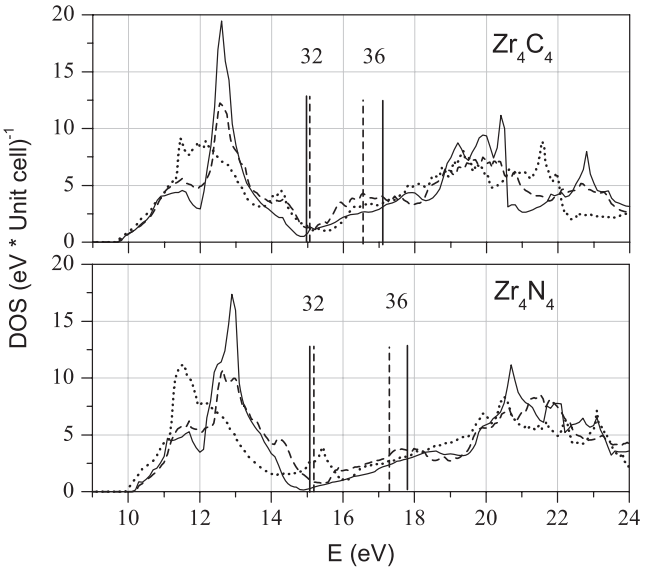

Figure 5. Densities of states (DOS) of cubic ($\gamma, \delta = 0$, ——) monoclinic ($\gamma = 0.27$, - - - -) and orthorhombic ($\delta = 0.15$, · · · · · ·) Zr_4C_4 and Zr_4N_4 phases. The vertical solid and dashed lines locate the Fermi energies associated with VEC = 32 (ZrC) and VEC = 36 (ZrN) in the cubic and monoclinic structures, respectively.

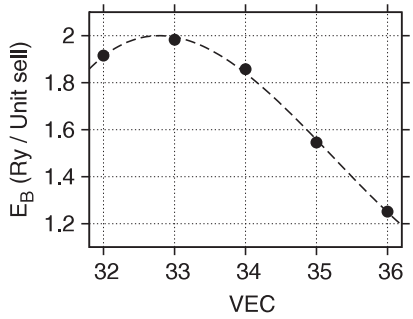

Figure 6. Band energy (E_B) of Zr_4C_4 at finite monoclinic strain ($\gamma = 0.27$) as a function of valence-electron concentration (VEC). The values of E_B are relative to the band energies of the unstrained crystals.

peaks of the DOS around E_{min} in ZrC and ZrN (cf figure 5). In the orthorhombic distorted ZrC–ZrN alloys, both peaks are present. On going from ZrC to ZrN, E_F crosses the additional peak above E_{min} and this correlates fairly well with a non-monotonic variation of E_B with composition.

We observe from figure 5 that the changes in the DOS caused by a monoclinic strain (equation (2)) are similar for ZrC and ZrN. In particular, the strain leads to an increase of the DOS just below and above E_{min}, and the DOS minimum at about 15 eV shifts towards higher energies. As a result, E_F is located at the high-energy slope of the strain-induced peak. For the distorted compounds, the states below and above E_{min} were found to be responsible for the positive and negative contributions to C_{44}, respectively. Indeed, monoclinic strain causes the redistribution of states from the main peak region towards the DOS minimum, which gives rise to an increase in the band energy E_B. The difference between the band energies of strained and unstrained alloys (ΔE_B) increases until the strain-induced states below E_{min} are occupied completely. In this case, the band structure contribution to the modulus C_{44} is positive. The maximum positive contribution is reached for a small increment in VEC (∼0.2–0.25) when E_F falls in the DOS minimum of the strained material. On the other hand, monoclinic strain also leads to a redistribution of states towards the bottom of the d band and to a lowering of the Fermi level. The contribution of these states to ΔE_B is negative. Consequently, with a further increase in VEC, E_B decreases. Hence, both the band energy and the modulus C_{44} will exhibit a maximum as a function of composition, which is confirmed by the results of the calculations of the band energy of the distorted ZrC as a function of VEC, as shown in figure 6. We note that this finding is consistent with the explanation for the composition dependence of C_{44} for TiC_xN_{1-x}, presented earlier in [13].

Using the calculated elastic moduli B, C_{11}, C_{12} and C_{44}, we estimated the moduli G and E and the Poisson ratio σ for ZrC_xN_{1-x} and $Zr_xTi_{1-x}C$. These quantities as functions of composition are displayed in figures 7 and 8, together with the experimental data from [6] for zirconium carbonitride alloys. For ZrC_xN_{1-x}, our results reproduce fairly well the experimental behavior of G and E with composition [6]. Our data show a distinct maximum at $x \sim 0.7$, in agreement with experiment [6]. However, we note that the theoretical characteristics G and E do not show local minima around $x = 0.3$, as seems to be observed experimentally (cf figure 7(a)), although due to the scattering in the experimental data, additional data collection may be required to draw a final conclusion on this apparent discrepancy. Comparing the data presented in figures 3 and 7(a), it is clear that the behavior of G and E are determined by the composition dependence of C_{44}. For B, we obtained a linear composition dependence. The computed $\sigma(x)$ curve shows a minimum around $x = 0.7$ (cf figure 8(a)). All these findings, obtained for ZrC_xN_{1-x}, speak in favor of a strength enhancement at intermediate compositions ($x \sim 0.7$–0.8) caused by the composition dependence of the C_{44} modulus.

For the elastic constants B, G and E of $Zr_xTi_{1-x}C$, a negative deviation from the mixing rule is observed at all compositions. Their composition dependence is monotonic and similar to the one predicted for C' and C_{44} (cf figure 3). These findings do not confirm the strength enhancement at intermediate compositions, as suggested from experiments [10].

4. Conclusion

An *ab initio* pseudo-potential methodology was applied to the calculation of the Gibbs free energy of mixing ΔG_{mix}, the bulk modulus B, the elastic constants C_{11}, C_{12} and C_{44}, the shear modulus G, the Young modulus E and the Poisson ratio σ of zirconium carbonitride and zirconium–titanium carbide alloys as functions of composition. For ZrC_xN_{1-x}, the predicted moduli revealed an extremum in their composition dependence, except for the $C' = \frac{1}{2}(C_{11} - C_{12})$ shear modulus that gradually increases with the valence-electron concentration, VEC. This extremum value of the

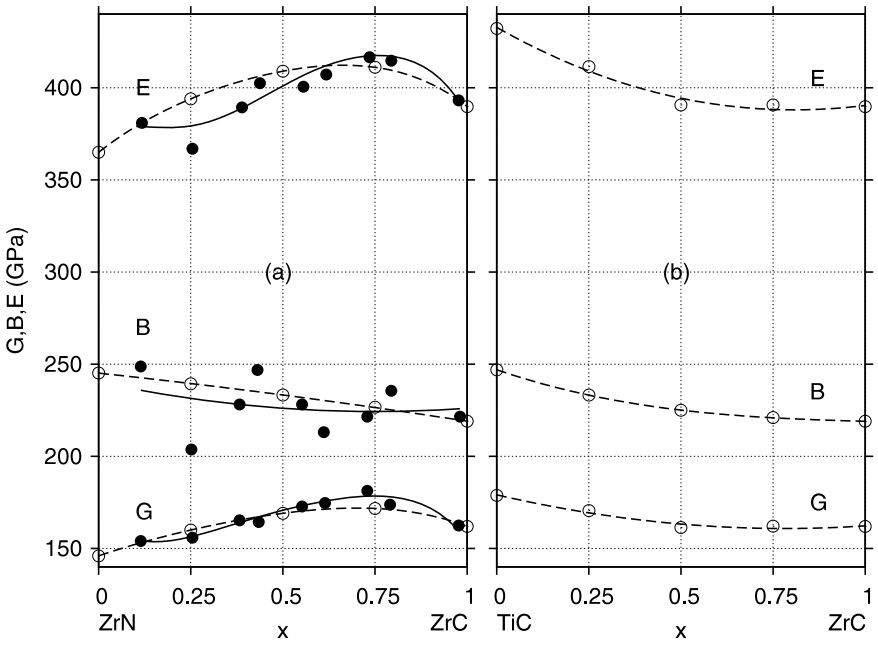

Figure 7. Calculated shear modulus (G), bulk modulus (B) and Young's modulus (E) for (a) ZrC_xN_{1-x} and (b) $Zr_xTi_{1-x}C$ (open circles) versus composition. The dashed curves are polynomial fits to the calculated data. The solid circles and solid lines are the experimental data and their interpolations, respectively, from [6].

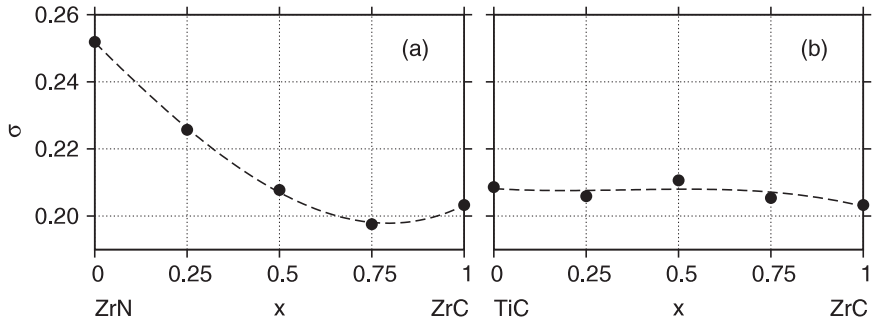

Figure 8. Poisson's ratio (σ) as a function of composition for (a) ZrC_xN_{1-x} and (b) $Zr_xTi_{1-x}C$.

elastic constants is entirely determined by that of the shear modulus C_{44} that shows a maximum value around VEC $\sim$ 8.2–8.3. The latter is related to specific changes in the band structure of ZrC_xN_{1-x} alloys induced by a monoclinic strain that determines the shear moduli C_{44}. In contrast to the carbonitrides, the elastic constants of ZrC–TiC alloys exhibit a monotonic composition dependence that can be attributed to the similarity of the band structures of the two carbides ZrC and TiC. The negative deviation of the elastic constants and the positive deviation of the lattice constants from the mixing rule as well as the positive formation energy over the entire composition range of the homogeneous $Zr_xTi_{1-x}C$ alloys indicate a weakening of the strength properties at intermediate compositions. The computed chemically spinodal and binodal decomposition curves show that face centered cubic (fcc) $Zr_xTi_{1-x}C$ solid solutions should undergo a phase decomposition into fcc ZrC and fcc TiC in a wide range of compositions and temperatures.

Acknowledgments

This work was supported by the STCU contract no. 4682. The work of P T has been performed under the auspices of the US Department of Energy by Lawrence Livermore National Laboratory under contract DE-AC52-07NA27344.

References

[1] Toth L E 1971 *Transition Metal Carbides and Nitrides* (New York: Academic)
[2] Storms E K 1967 *The Refractory Carbides* (New York: Academic)
[3] Lengauer W 2000 *Transition Metal Carbides, Nitrides and Carbonitrides* (*Handbook of Ceramic Hard Materials* vol 1) ed R Riedel (Weinheim: Wiley-VCH)
[4] Mayrhofer P H, Mitterer C, Hulttman L and Clements H 2006 *Prog. Mater. Sci.* **51** 1032

[5] Lengauer W, Binder S, Aigner K, Ettmayer P, Guillou A, Debuigne J and Groboth G 1995 *J. Alloys Compounds* **217** 137
[6] Yang Q, Lengauer W, Koch T, Scheerer M and Smid I 2000 *J. Alloys Compounds* **309** L5
[7] Bilyk I I 1972 *Powder Metallurgy* **6** 49
[8] Jangg G, Kieffer R and Usner L 1968 *J. Less-Com. Met.* **14** 269
[9] Kieffer R, Nowotny H, Ettmayer P and Usner L 1968 *Monatsh. Chem.* **99** 1020
[10] Kovalsky A E and Petrova L D 1951 *Microtverdost* (Moskow: Academy of Science of USSR)
[11] Zhukov V P, Gubanov V A, Jepsen O, Christensen N E and Andersen O K 1988 *Phil. Mag.* B **58** 139
[12] Jhi S-H and Ihm J 1997 *Phys. Rev.* B **56** 13826
[13] Jhi S-H, Ihm J, Louie S G and Cohen M L 1999 *Nature* **399** 132
[14] Ivashchenko V I, Turchi P E A, Gonis A, Ivashchenko L A and Scrynsckyy P L 2006 *Metall. Mater. Trans.* **37A** 3391
[15] Baroni S *et al* http://www.pwscf.org
[16] Vanderbilt D 1990 *Phys. Rev.* B **41** 7892
[17] Perdew J P, Burke K and Ernzerhof M 1966 *Phys. Rev. Lett.* **77** 3865
[18] Monkhorst H J and Pack J D 1976 *Phys. Rev.* B **13** 5188
[19] Murnaghan F D 1944 *Proc. Natl. Acad. Sci. USA* **30** 244
[20] Mehl M J 1993 *Phys. Rev.* B **47** 2493
[21] Cheng D, Wang S and Ye H 2004 *J. Alloys Compounds.* **377** 221
[22] Wu Z, Chen X-J, Struzhkin V and Cohen R E 2005 *Phys. Rev.* B **71** 214103
[23] Chen X-J, Struzhkin V V, Wu Z, Somayazulu M, Qian J, Kung S, Christensen A N, Zhao Y, Cohen R E, Mao H and Hemley R J 2005 *Proc. Natl Acad. Sci. USA* **102** 3198
[24] Knotek O and Barimani A 1989 *Thin Solid Films* **174** 51
[25] Christensen A N, Dietrich O W, Kress W and Teuchert W D 1979 *Phys. Rev.* B **19** 5699
[26] Chang R and Graham L J 1966 *J. Appl. Phys.* **37** 3778
[27] Weber W 1973 *Phys. Rev.* B **8** 5082
[28] Ahuja A, Eriksson O, Wills J M and Johansson B 1996 *Phys. Rev.* B **53** 3072
[29] Choy M M, Cook W R, Hearmon R F S, Jaffe H, Jerphagon J, Kurtz S K, Liu S T and Nelson D F 1979 *Elastic, Piezoelectric, Pyroelectric, Piezooptic, Electro-optic Constants and Nonlinear Dielectric Susceptibilities of Crystals* (*Landolt-Borstein, Numerical Data and Functional Relationship in Science and Technology* vol 11) ed K-H Hellwege and A M Hellwege (Berlin: Springer)
[30] Pintschovius L, Reichardt W and Scheere B 1978 *J. Phys. C: Solid State Phys.* **11** 1557
[31] Gilman I J and Roberts B W 1961 *J. Appl. Phys.* **32** 1405